Chapter 13

Numerical Analysis on the Simulated Heavy Rainfall Event of Tropical Cyclone Fung-Wong

Lei-Ming Ma and Xu-Wei Bao

Additional information is available at the end of the chapter

http://dx.doi.org/10.5772/intechopen.72264

Abstract

During landfall on the southeast coast of China, tropical cyclone (TC) Fung-Wong in the year 2008 caused torrential rainfall and flooding. In order to clarify the mechanism for the rainfall, a series of numerical simulations were conducted in this study using the National Center for Atmospheric Research (NCAR), Weather Research & Forecasting (WRF) mesoscale numerical model with three-nested domains and a highest horizontal resolution of 600 m. Numerical analysis was then performed based on the simulations. It is found that, during the evolution of heavy rainfall, quasi-frontal systems are frequently produced at the boundary of TC inflow and convective updrafts, which is more evident at the region of TC inner core and spiral rain band. The existence of energy cascading, featured by the energy transition among TC-scale inflow and convective cells, is also identified at the quasi-frontal region. These multiscale processes of Fung-Wong are further clarified by the analysis of helicity, which are believed to be responsible for the genesis and development of deep convection and rapid accumulation of rainfall. In the quasi-frontal region, numerical analysis further indicates the existence of intensive low-level wind shear as well as vertically turning of low level jet (LLJ), implying the contribution from Kelvin-Helmholtz instability (KHI).

Keywords: tropical cyclone, rainfall, landfall, helicity, CAPE

1. Introduction

Tropical cyclones (TCs) are the most devastating weather systems. Along with the direct threat from the strong winds, hazards are often brought by the torrential rainfall that causes flood and landslide. Previous studies on TC rainfall either focused on the structure and dynamics of secondary eyewalls [1] and principal rainbands [2] within the inner core or mesoscale effects such as orographically forced ascent (upslope) and coastal front in predecessor rain events

(PREs) [3]. In addition to that of TCs, suggested rainfall genesis mechanisms also include the convergence of moist outflows from previous cellular convection [4], squall line at the advance of moist cold pools [5], unorganized thermodynamic-generated tropical deep convections [6], etc. Among them, cold pools which are areas of evaporatively cooled downdraft air that spread out beneath precipitating cloud [7] have been frequently investigated because of its prominent role in growth of convection. In TCs, although cold pools are less common due to the relative lack of dry air in comparison to that in midlatitudes, they are known to be the primary mechanism for the sustenance of multicell thunderstorms and convective lines [8]. While TC outer rainband formation has been attributed to a variety of processes, including outward propagating inertia-gravity waves [9] and vortex-Rossby waves [10], it seems plausible that the cold pool played a contributory role in the intensification of TC outer rainband. Numerous TC studies [11–13] have utilized coastal buoys, instrumental towers, and aircraft data to document outer rainband and cold pool structure. When observed, cold pools are often associated with outer rainbands or bands adjacent to inward-spiraling dry air intrusions. These studies also noted decreasing storm-relative inflow, decreasing equivalent potential temperatures, and locally enhanced wind speeds in the boundary layer beneath the rainbands. Moreover, while a necessary condition for cold pool formation may be the presence of midlevel dry air, cold pool intensity appears more related to factors other than the degree of midlevel dryness. While affecting the growth of rainfall, cold pools are sometimes associated with cold fronts and cold air damming (CAD) [14]. Atallah and Bosart [15] examined aspects of the precipitation distribution of hurricane Floyd (1999) through synoptic and modeling analyses and found that precipitation ahead of Floyd's track was generally enhanced along the cold front from approximately 12 h before the time of storm passage. CAD occurs most often on the eastern side of approximately north-south-oriented mountains, as cold air moving toward the eastern slopes has insufficient kinetic energy to go over the barrier and is then forced to decelerate. The genesis of cold pool can be associated with extratropical transition (ET) [16–18], which occurs from a warm-core to cold-core cyclone and gains extratropical cyclone characteristics. Snodgrass et al. [19] found that the heaviest convective rainfall occurred in mesoscale arcs around cloud-free areas, reminiscent of outflow boundaries of cold pools created by earlier convection. However, different with the mechanism of cold pool, Tompkins [6] shows that air moistened by evaporating precipitation can be pushed outward by a drier downdraft driven by precipitation and trigger new convection when the surface air becomes sufficiently buoyant.

As the development of TC rainfall becomes quite complicated during landfall due to the interaction with midlatitude atmospheric systems and the topographical effect, these complicated processes were usually investigated with advanced atmospheric numerical models based on a series of dynamic and thermodynamic equations. TC rainfall mechanism can then be further understood with the assistance of dynamic or thermodynamic diagnosis. In this study, the mechanism of heavy rainfall associated with the frontal structure and cold pool during the landfall process of TC Fung-Wong (2008) is preliminarily examined based on the numerical simulations and numerical analysis with the special use of multiscale conception of helicity [20, 21]. The original definition of helicity [22] has been frequently employed to investigate the structure of convections and TCs [23–25]. Wu et al. [26], by investigating the relationship

http://dx.doi.org/10.5772/intechopen.72264

between helicity and nonlinear energy transition with a helicity budget of the mean and disturbance flows, indicated that the helical mean flow transfers helicity to the convective eddies and both the buoyant effect and mean-eddy exchange are important sources for disturbance. It is further indicated that the disturbances gain helicity from mean flows and the buoyancy effect amplifies it. Fei and Tan [24] reported that weak helicity is favorable for the energy cascading from large scale to convective scale at the early stage of a convective storm. Hendricks et al. [25] and Montgomery et al. [27] argued that vertical hot towers (VHTs), helical by definition because of coincident updrafts and vertical vorticity, were the preferred mode of convection in TCs. Molinari and Vollaro [28] also identified convective cells, generally favored downshear, would be stronger and longer-lived as a result of larger helicity. Although it is widely accepted that intensive helicity favors the genesis of supercell and TC intensification, it is still an open question of the connection between helicity and the evolution of TC heavy rainfall. In this regard, the mechanism for the rapid growth of TC Fung-Wong's heavy rainfall is examined based on the understanding of Fung-Wong's multiscale processes analyzed with helicity.

TC Fung-Wong, as the first strong typhoon made landfall over China mainland in 2008, was characterized by torrential rainfall, large size, and wide-range influence. It was developed at 06 UTC, 25 July 2008, over the Northwest Pacific and then intensified into a typhoon at 09 UTC, 26 July. From the morning on 27 July, it started to move northwest and approached the east coast of Taiwan Island. Fung-Wong intensified into a severe typhoon at 12 UTC, 27 July. As shown on the FY2C satellite imagery, the cloud distribution of Fung-Wong was significantly asymmetric before the occurrence of landfall. More clouds were clustered to the southwest of TC. A clear eye formed before it reached Taiwan. At 22 UTC, 27 July, Fung-Wong landed on Hualian, Taiwan, with the maximal wind speed of 45 m s^{-1} near its center. As Fung-Wong passed over Taiwan, heaviest rainfall of 818 mm was recorded near Tai-Ping Mountain. Fung-Wong landed again on Donghan, Fujian province, at 14 UTC, 28 July, with the estimated maximal wind speed of 33 m s^{-1} near its center. At that time, NASA's CloudSat satellite's Cloud Profiling Radar showed that the cloud top of Fung-Wong reached more than 15 km with estimated precipitation rate exceeding 30 mm h^{-1} on 28 Jul. After the second landfall, it was quickly reduced to a severe tropical storm, and its eyewall and spiral structure were significantly vanished. However, during its stay inland for about 52 h, it produced heavy rainfall in Zhejiang and Fujian province, leading to two rivers flooding, with an estimated total loss of CNY 3.37 billion.

To clarify the mechanism for heavy rainfall, it is helpful to carry out high-resolution simulation with mesoscale nonhydrostatic microphysical models. Recent numerical experiments using the Weather Research & Forecasting (WRF) model have shown some promise in forecasting TCs near landfall [29]. In this study, numerical experiments were designed and performed with the multiply-nested WRF model. With an inner resolution of 600 m, it provides the possibility for answering questions on the role of the energy cascading on the rainfall development of TCs.

The methods and data are described in Section 2. The numerical simulations on track, intensity, and rainfall of Fung-Wong are verified in Section 3. The numerical analysis on the multiscale mechanism of the heavy rainfall is conducted in Section 4. Section 5 is the summary.

2. Methodology

2.1. Numerical experiments

In order to clarify the multiscale mechanism for heavy rainfall, high-resolution numerical experiments were conducted with the NCAR/WRF mesoscale model [29]. The triply nested model domains (**Figure 1a**), i.e., the outermost domain (D1), the inner domain (D2), and the innermost domain (D3), are designed with horizontal spacing of 15 km, 3 km, and 600 m, respectively, with domain sizes of 281 × 281, 721 × 721, and 721 × 721 grid points, respectively. D1, which covers the northwest Pacific, eastern Tibetan plateau, Bengal Bay, and China, is employed to examine the large-scale environmental flow. D2, which covers east China, is one-way nested within D1 and is used to examine the major landfall processes. D3, which is fixed and one-way nested within D2, is used to analyze the detailed structure of rainfall system. A total of 37 vertical sigma levels are used for all the domains. The Kain-Fritsch cumulus parameterization scheme [30] with modification of convection trigger function [31] is used in D1. However, in D2 and D3, no cumulus parameterization scheme is considered to avoid its ambiguous application in high-resolution simulation. The WRF single-moment 6 (WSM6) class multiphase cloud scheme is employed in all domains to represent cloud physics. The Yonsei University (YSU) planetary boundary layer (PBL) scheme [32], using counter-gradient terms to represent nonlocal fluxes, is considered for PBL parameterization in D1 and D2. The YSU PBL scheme [33, 34] explicitly treats the entrainment layer at the PBL top with the surface buoyancy flux in line with results from large-eddy models. The PBL top is defined using a critical bulk Richardson number of zero. The turbulent kinetic energy (TKE) diffusion scheme is employed in D3 to deal with the PBL physics [35]. Furthermore, the rapid radiative transfer model (RRTM) scheme [36] and Dudhia scheme [37] are used for the parameterization of longwave and shortwave radiation, respectively.

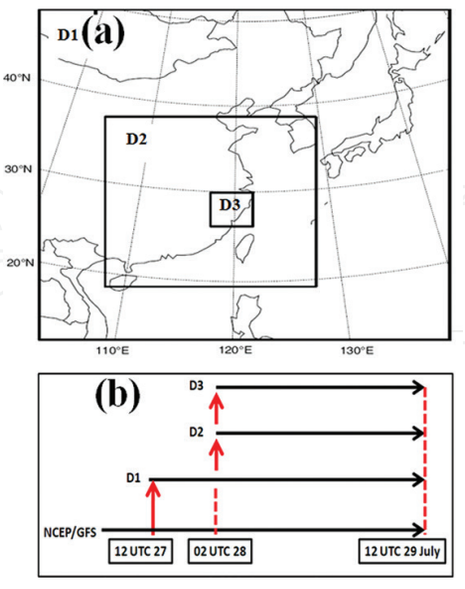

Figure 1. (a) The triply nested model domains for numerical simulation (D1, the outermost domain; D2, the inner domain; D3, the innermost domain) and (b) the phases of model integration for each model domain.

Figure 1b indicates the phases for model integration in each domain. For domain D1, the time between 12UTC, 27 July, and 12UTC, 29 July, is chosen for an overall description of Fung-Wong's track and rainfall during landfall. In order to examine the detailed evolution of TC structure and rainfall, the time between 02UTC 28 and 12UTC 29 is selected for D2, and the time between 02UTC 28 and 12UTC 28 is selected for D3. The background field of D1 is interpolated from the analysis of NCEP Global Forecast System (GFS) whose horizontal resolution is 0.5°. The vortex initialization scheme developed by Ma and Tan [38] is employed to produce the initial analysis for TC simulation. In this scheme, sea level pressure (SLP) derived from satellite sea surface wind is used to generate the initial TC circulation. To ensure a reasonable simulation of Fung-Wong's track and intensity, two numerical experiments, e.g., Expt. CTRL (the one without vortex initialization) and Expt. VIRV (the one with vortex initialization), are conducted. The 3B-42 gridded rainfall datasets with the resolution of 0.25 × 0.25°, derived from the Tropical Rainfall Measuring Mission (TRMM), are employed for verification on rainfall simulation.

2.2. The multiscale conception of helicity

Helicity ($H = \vec{V} \cdot \vec{\omega}$) is originally defined as the scalar product of velocity ($\vec{V}$) and vorticity vector ($\vec{\omega} = \nabla \wedge \vec{V}$), which represents the rotational characteristics in the motion direction and the twining structure of the vortex tubes [39]. Subsequent researches [20, 21] further examined its multiscale conception.

According to Tan and Wu [20], for large-scale motion, helicity (hereafter H_1) can be approximated as

$$H_1 \approx -u\left(\frac{\partial v}{\partial z}\right) + v\left(\frac{\partial u}{\partial z}\right) \tag{1}$$

Based on the assumption of thermal wind balance, H_1 can be further expressed as

$$H_1 \approx -u\frac{\partial \theta}{\partial x} + v\frac{\partial \theta}{\partial y} = -\vec{V} \cdot \nabla \theta \tag{2}$$

where θ is the potential temperature.

Clearly, Eq. (2) indicates the equality between helicity and temperature advection for large-scale flow, e.g., helicity should be positive (negative) for warm (cold) air advection. Therefore, very large gradient of helicity is associated with frontogenesis.

For small-scale motion, helicity (hereafter H_2) can be rewritten as

$$H_2 \approx u\frac{\partial w}{\partial y} - v\frac{\partial w}{\partial x} + w\left(\frac{\partial v}{\partial x} - \frac{\partial u}{\partial y}\right) \tag{3}$$

Assuming $\alpha = \alpha(z)$ the angle between velocity vector $\vec{v}$ ($|\vec{v}|^2 = u^2 + v^2$) and its component u (i.e., $\tan\alpha = \frac{v}{u}$), then

$$H_1 \approx v^2\frac{\partial}{\partial z}\left(\frac{u}{v}\right) = -|\vec{v}|^2\frac{\partial \alpha}{\partial z} \tag{4}$$

The multiscale conception of helicity discussed above is fundamental for the understanding of energy cascade, which occurs either by Taylor's mechanism of stretching and spin-up of small-scale vortices due to large-scale strain or twisting of small-scale vortex filaments due to a large-scale screw.

3. Numerical experiments on TC landfall process and evolution of rainfall

The landfall process of Fung-Wong is simulated based on the experiments in Section 2. Statistical variables, including the errors of track and intensity, are calculated. The result indicates that the errors in the experiment VIRV are generally less than CTRL. For example, the errors of 24 h simulated track for the experiments CTRL and VIRV are 79 and 54 km, respectively. The improvement in TC intensity is about 27.6% in the simulation of maximum wind speed (MWS) and 16.4% in minimum sea level pressure (MSLP), respectively. Because of the "spin-up" process of numerical simulation, both the experiments exhibit smaller MWS and MSLP errors at 24 h than 12 h. However, the difference of MSLP between VIRV and CTRL increases with the model integration, indicating that the simulation of MSLP is sensitive to the initial condition. For the rainfall simulation (**Figure 2**), the rainfall pattern in VIRV agrees with the TRMM observation. In this regard, the results from VIRV simulations are used for the analysis of rainfall mechanism in the subsequent section.

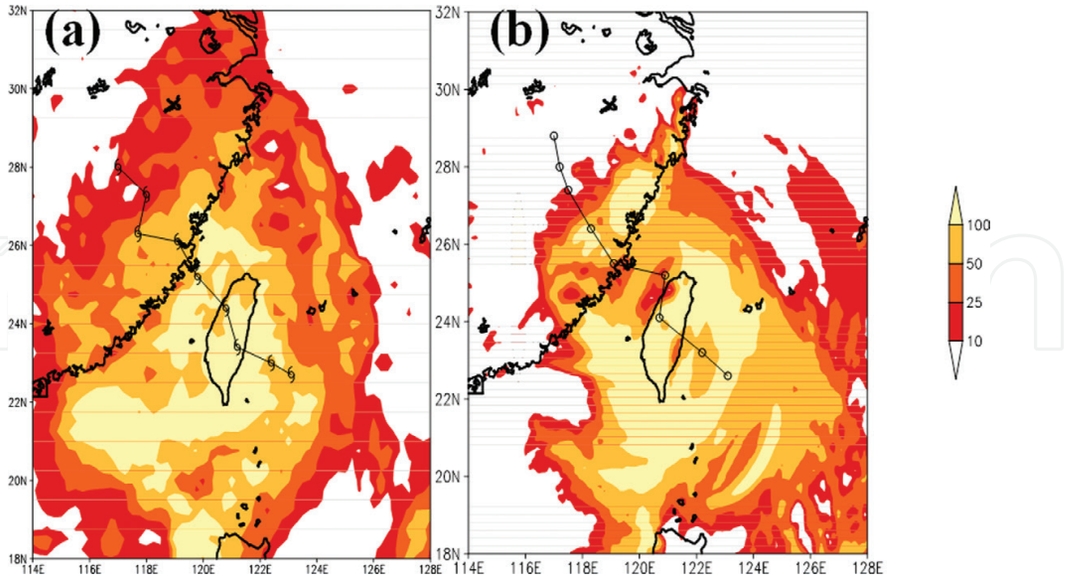

Figure 2. The accumulated rainfall (mm) during 12UTC 27–12UTC 29, Jul 2009, from TRMM 3B42 (a) and numerical simulation from D1 (b).

4. Numerical analysis on the multiscale systems associated with the torrential rainfall

4.1. Quasi-frontal structure viewed from helicity, low-level jet (LLJ), and cold pool

Numerous studies have highlighted the role of preexisting boundaries intersecting the primary convective system where cyclonic-only mesovortices were observed to form at the intersection point [40, 41]. More detailed analysis also indicated shearing instability [42] as the genesis mechanism for cyclonic-only low-level vortices formed along mesoscale boundaries such as gust fronts [43, 44]. These mesoscale boundaries are usually associated with frontal structures, which are required to be examined to clarify the mechanism of heavy rainfall. While it has long been recognized that the low-level jet (LLJ) is an efficient moisture transport mechanism [45] and a source of large-scale destabilization through warm advection [46, 47], the frontogenetical character of the boundary of LLJ can be important for the genesis of MCSs [48]. Therefore, the frontogenesis process similar to that of Augustine and Caracena [49] is investigated here to understand the characteristics of boundaries associated with MCSs. In particular, a time-averaged composite vertical cross section at 6 h preceding the mature stage shows that the LLJ in the plane of the cross section ascending the northeastward sloping frontal surface. Trier et al. [50] argued that long-lived MCSs are aided by the frontogenetical lifting of air by the LLJ, which produces a zone of elevated conditional instability favorable for rainfall genesis.

Through the analysis on the evolution of H_1 during TC landfall, this study also identifies that relative warm and moist LLJs associated with TC inflow frequently appear and move toward the TC core region and finally meet with the strong cold convective downdrafts which was induced by the convective detrainment from the middle-to-upper troposphere (PBL, **Figure 3**). As a result, quasi-frontal structure is generated at the boundary between the warm LLJ and cold downdraft. The LLJ intensifies as the front gradually sharpens. The large curvature near the quasi-front should serve to accelerate the buoyant air and the growth of convection. According to Eq. (4), the vertical shear of the angle between vector $\vec{v}$ and u component is equivalent to the ratio between helicity (H_1) and the square of total horizontal velocity. In this regard, positive helicity should be generated when the LLJ turns clockwise with height. It is interesting to find that before the occurrence of heavy rainfall, the shear vector of LLJ generally turns counterclockwise with height ($\frac{\partial \alpha}{\partial z}$ is positive). This relation indicates the existence of negative helicity and cold advection. However, as heavy rainfall occurs, the shear vector turns clockwise with height, showing a positive helicity. It is also noticed that high potential vorticity (PV, >2.5 PVU) associated with the mesoscale disturbances mainly occupies 700–950 hPa before the genesis of heavy rainfall. These PV disturbances then grow rapidly and extend to the whole troposphere, in companion with the genesis of heavy rainfall. Moreover, to evaluate the influence of the frontogenetical forcing on the growth of heavy rainfall, the Sawyer-Eliassen equation is further calculated. It is found that evident frontogenetical forcing (stream function value is −10.1 hPa m s^{-1}) is formed at the quasi-frontal area to the southeastern part of heavy rainfall. The forcing is intensified (−12.2 hPa m s^{-1}) and extended from 400 hPa to a lower level (700 hPa) at the peak time of rainfall (04UTC 28 Jul).

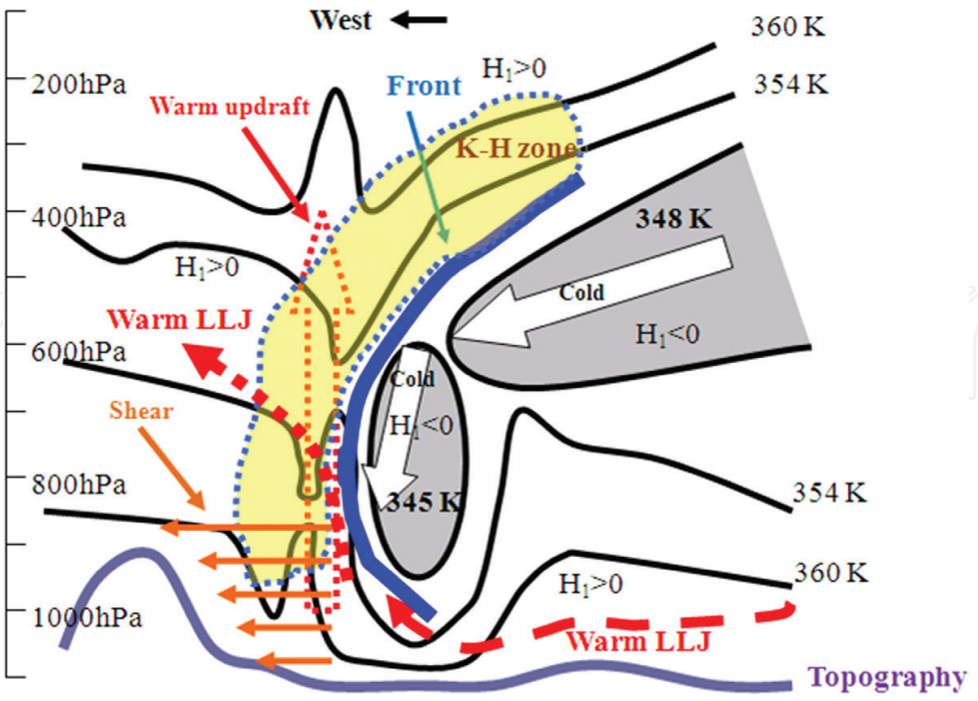

Figure 3. Schematic diagram of the multiscale quasi-frontal structure that results in the heavy rainfall.

Studies on tropical convection [51–53] suggested that convective rainfall rate is directly related to cold pool intensity. A number of idealized numerical simulations of tropical [54] and mid-latitude [55, 56] convection also have shown that cold pool may intensify when the low- to mid-level moisture is drier. Here, this study explores such relationship based on the simulation for Fung-Wong's inner rainbands where the most intensive rainfall appears. It is found that maximum $\Delta\theta$ deficits ranged from 1 to 5 K with a mean value of 2.7 K, while maximum $\Delta\theta_e$ deficits ranged from 1 to 14 K with a mean of 6.2 K. Thus, Fung-Wong's cold pools which lead to the heavy rainfall was equally intense as cold pools observed in other tropical storms. Moreover, in the cross-band direction, convergence of strong storm-relative inflow along the cold pool leading edge was coincident with a modest meso-high pressure anomaly, while inflow divergence prevailed through the collocated rainfall and cold pool maxima (figure is not given). Such structure is qualitatively consistent with many prior studies of TC outer rainbands and their associated cold pools [11, 12, 53]. In the along-band direction, several cold pools show signs of upband expansion while being advected downband by the prevailing cyclonic flow.

Meanwhile, the simulated wind profiles at the site of the most intensive cold pool exhibited easterly surface winds that veered with height, with 0–6 km shear vectors oriented toward the north at ~13 m s^{-1}. The strength and orientation (primarily crossband) of the 0–3 km shear vectors were marginally consistent with expectations for intense, long-lived rainbands [57]. Simulations further indicate a shallow moist layer near the surface (below ~1 km), drier air at mid-levels (~2–6 km), and moister air aloft. The midlevel RH minima approached 30–35% near 3–5 km AGL.

According to previous studies, the physical mechanisms for the genesis of this kind of cold pool include (1) advection of cooler and drier air from over land, (2) enhancement of rainband convection over land leading to mesoscale saturated downdrafts of cool and dry

http://dx.doi.org/10.5772/intechopen.72264

middle-level air, (3) enhanced turbulent entrainment of dry air from above the top of PBL, and (4) loss of the oceanic heat and moisture source, causing air to cool dry adiabatically while flowing toward the center. In this study, the first mechanism seems the most plausible if one examines the temperature advection disclosed by large-scale helicity. In contrast, the second mechanism seems not considerable, as the cold air is not covered by the rainband as seen from the FY2C cloud image. Based on the analysis of the simulations, the other two mechanisms should have played an additional indirect role in inducing the cold flow in the middle level.

4.2. K-H instability associated with the multiscale systems

According to Romine and Wilhelmson [58], the Kelvin-Helmholtz instability is one of the principle mechanisms that result in the genesis of spiral rain band. Based on radar data, Weckwerth and Wakimoto [59] examined a mesoscale front in association with the outflow produced by the downdraft of a supercell. They found that the K-H instability and mesoscale convective cell develop at the top of the edge of front. Detailed investigation on the important features of the quasi-frontal structure, e.g., vertical wind shear, local Richardson number (less than 1/4), and the distribution of wave structure, which is parallel to the gust-front head and perpendicular to the low-level shear vector, shows high similarity with the characteristics of K-H waves from supercells [59] and hurricanes [58]. It is also noticed that the quasi-frontal region is characterized by vertical vorticity maxima. According to Atkins and Laurent [60], as the vorticity near the front can be amplified by updraft through stretching, the vorticity maxima provides favorable locations for the growth of instability and convection. These convective cells subsequently propagated back relative to the outflow boundary while they preferentially existed along the updraft side of the K-H waves. The spacing of the cells at the leading edge of the outflow boundary, particularly along the northern part, is approximately 5 km, which compares well with the wavelength of the K-H waves. It also indicates that the static instability increases and ultimately triggered upward motion at the front. As a result, horizontal shear of vertical motion across the front develops and contributes to the growth of helicity and helical disturbance. It is also recognized that the intersections between the vortex tubes at the gust-front head are characterized by vertical vorticity maxima. In addition to the K-H instability, this study also calculated the Brunt-Vaisala frequency atop the radial inflow layer at the spiral rainband and the decrease of Scorer number [61] with height below the cold flow, which indicates the presence of gravity wave with the wave period of 220 s. It thus may mix the dynamic-unstable sheared layer and contribute to the accumulation of rainfall [58].

4.2.1. Numerical analysis on energy cascading

The vertical wind profile averaged at the quasi-frontal region is further investigated. It is found that the profile is characterized with clockwise-turning and increased curvature of hodograph through a deep layer. According to Wu et al. [26], the increased curvature of hodograph is beneficial to the development of small-scale convection due to the energy cascading from the basic flow. In this regard, the process of energy cascading is further examined based on the numerical simulation results.

Using the conception of difference in total energy (DTE), Tan et al. (hereafter T04) [62] examined the impacts of initial small-scale disturbance on a "surprise" snowstorm through the analysis of energy cascading. Similar to the definition of DTE by T04, the total energy (*TE*) is defined here by considering kinetic and internal components:

$$TE = \frac{1}{2}\left(U_{i,j,k}{}^2 + V_{i,j,k}{}^2 + kT_{i,j,k}{}^2\right) \tag{5}$$

where U, V, and T are horizontal u-wind, v-wind components, and temperature, respectively. $k = C_p/T_r$ (the reference temperature T_r =287 K). I, j, and k are the numbers of x, y, and σ grid points, respectively.

A power spectrum of *TE*, averaged in the region of heavy rainfall, is analyzed. Wavenumbers 0, 1, and 2 are the TC scales following Krishnamurti et al. [63]. Meanwhile, the scales of the individual deep convective clouds reside around the azimuthal wave numbers 20–30. According to Saltzman [64], the TC scale is about several hundreds of kilometers, whereas the scale of convection, including updrafts and adjacent downdrafts, is only a few kilometers. It shows that a sizeable portion of the variance of *TE* is contributed by the first few harmonics (0–4) in the innermost region. The contribution from wavenumbers 3 to 55 (associated with medium- to small-scale processes) accounts for less than 10% of total *TE*, which agrees with the results from quasi-geostrophic models [65].

To better understand the energy transition during rainfall, this section further examines the relation between helicity, the magnitude of which is associated with kinematic energy, and CAPE, an indicator of potential energy. Krishnamurti et al. [63], by examining the scale interaction of hurricane inferred from the decomposition of the liquid water mixing ratio fields, found that nonlinear interaction of kinetic energy and available potential energy among cloud scales and the hurricane scale provide the energy to drive the hurricane. The generation of available potential energy and its transformation to kinetic energy takes place directly on the larger scales of the hurricane. Their results among hurricane scales and smaller scales show largely a cascade of energy, that is, hurricane scales lose energy when they interact with other scales.

The evolution of CAPE and helicity of TC circulation during landfall (12UTC 27–12UTC 29 July) is investigated. It shows that an approximated negative correlation exists between H_1 and CAPE before the occurrence of rainfall, which is mainly featured by the decrease (increase) of CAPE (H_1). However after rainfall, the original negative relation is replaced by an approximate positive correlation, which decreases simultaneously. The decrease of CAPE should be associated with the significantly reduced heat flux from land surface and the large consumption of CAPE during the rainfall process. Scatter plot also shows that intensive H_1 corresponds to low CAPE (e.g., CAPE of 3500 J kg^{-1} vs. H_1 of 50–150 m^2 s^{-2}) during the growth of convection. In other words, kinematic energy increases as potential energy is consumed. However, there is no clear correlation between CAPE and H_2, indicating that the energy from CAPE might not directly fuel the growth of small-scale convection. Moreover, over the land, H_1 is positive in more than 66.6% of the rainfall region. The maximum of CAPE is 3500 J kg^{-1} with H_1 of 50–150 m^2 s^{-2}. Five percent of H_1 are greater than 400 m^2 s^{-2}, with the biggest of 800 m^2 s^{-2}. Over land, more than 95% of H_1 is positive, with H_1 decreasing with CAPE. Most of the intensive H_1 corresponds to CAPE less than 500 J kg^{-1}, while over the ocean, negative H_1 corresponds to the CAPE as low as 1000 J kg^{-1}.

The nonlinear multiscale transition of energy from basic flow to the process of disturbance (E_t) can be also represented by $E_t = -u'w'\partial\overline{u}/\partial z - v'w'\partial\overline{v}/\partial z$ (hereafter WL92) [26]. Here E_t represents the weakening phase of environmental vertical wind shear by convection, during which larger-scale instability is eliminated by the small-scale motion. Similar to WL92, this study examined the difference of E_t produced by D1 and D2. It shows that the E_t produced by D1 is generally higher than that of D2, with the difference more evident after landfall, and the E_t of D1 rapidly decreases. The amplitude of energy transition in D2 increases persistently as the typhoon makes landfall, which might relate to the development of small-scale convection. It is also noticed that the tendency of E_t evolution is nearly in positive correlation with H_2 (instead of H_1). The distribution of E_t is examined before and after the heavy rainfall, during which the maximas of E_t merged together, in concert with the rainfall intensification.

Detailed analysis also shows that the largest value of the generation of available potential energy (CAPE) and its conversion to kinetic energy occurs at the region of the heaviest rain in the simulation of TC Fung-Wong. The values decrease rapidly from TC core region to the outer radial belts. The cloud scales essentially extract energy from the TC scale (azimuthally averaged wavenumber 0) system. It implies that the TC scale is barotropically unstable to the cloud scales (wavenumbers 1 and 2). This is essentially a cascading process where energy is conveyed from the larger to the smaller scales. The generation of available potential energy and its transformation to kinetic energy takes place directly on the larger scales of TC Fung-Wong. Using a spectral closure calculation, Andre and Lesieur [66] showed that transport of energy through the inertial range is sensitive to the presence of helicity. In the calculations of this study, the time evolution of the energy spectrum toward the $k^{-5/3}$ form is slowed down when helicity is injected at small wavenumbers. It thus supports the argument by Tsinober and Levich [67] that helical structures might be an inherent part of the turbulent energy cascade and thereby suppress the nonlinear terms responsible for the cascade.

5. Summary and discussion

High-resolution simulations are performed with nonhydrostatic WRF mesoscale numerical model to clarify the multiscale mechanisms leading to the heavy rainfall of TC Fung-Wong during landfall on southwestern coast of China. Numerical analysis shows that quasi-frontal structures are frequently generated at the boundary of warm LLJs associated with TC inflow and cold convective downdrafts, which favor the genesis of intensive rainfall. Some important features of the quasi-frontal structures, e.g., intensive vertical wind shear and small local Richardson number, exhibit similarity with that of K-H waves from supercell. The hodograph of LLJ which turns clockwise with height tends to produce positive helicity and favors the genesis of convection. An evident antiphase relationship between H_1 and CAPE during heavy rainfall suggests the energy transition from CAPE to kinematic energy.

For the future study, the structure, organization, and impact of convective rainfall systems in TCs during landfall remain a fruitful area for research. Convective cells are known to be favored downshear in TCs due to the shear-induced increase in convergence and upward motion downshear [68]. The variations of helicity and CAPE described in this paper should

also connect with vertical shear. As has been stated by Molinari and Vollaro [28], the helicity and CAPE in the presence of large ambient shear exceeded those in storms with small ambient shear. The reduction in stability and increase in helicity might represent the positive influence of large vertical wind shear in offsetting the greater ventilation of the storm core. Many questions about heavy rainfall in landfalling TCs remain unanswered. How about the multiscale characteristics of helicity in different situation of shear? How do the multiscale helicity affect supercells of TCs? Observation (i.e., radar) and simulations are required to confirm the processes that such cells develop in landfalling TCs. Moreover, the detailed cascading process of rainfall should be carefully examined based on energy budget. The quantitative impact of systems in various scales on rainfall deserved to be examined with sensitive numerical experiments. Additional studies should be conducted to verify and expand upon the limited observation of cold pool associated with landfalling TCs. In particular, combination of numerical simulation and datasets including both onshore and offshore observations at various intensities and evolutionary stages across a spectrum of large-scale environments would improve understanding of cold pools and their various feedbacks on convection. To enhance the simulation on cold pools, improved representation of microphysics in models would also be beneficial. Furthermore, although the orographic effect is not addressed in this study as there is no clear evident of relationship between the terrain and the amplification of rainfall, the alteration, or reorganization of the convective clouds, frontal systems associated with TC when it encounters topographic features might be possible [69], which will be examined in a next study.

Acknowledgements

This research was jointly supported by the National Science Foundation Project (no. 41475059) and China Key Research and Development Program (no. 2016YFC0201900).

Author details

Lei-Ming Ma[1,2]* and Xu-Wei Bao[3]

*Address all correspondence to: malm@mail.typhoon.gov.cn

1 Shanghai Meteorological Center, Shanghai, P. R. China

2 Shanghai Key Laboratory of Meteorology and Health, Shanghai, P. R. China

3 Shanghai Typhoon Institute, Shanghai, P. R. China

References

[1] Houze RA Jr et al. The Hurricane rainband and intensity change experiment: Observations and modeling of Hurricanes Katrina, Ophelia, and Rita. Bulletin of the American Meteorological Society. 2006;**87**:1503-1521

[2] Hence DA, Houze RA Jr. Kinematic structure of convective-scale elements in the rainbands of Hurricanes Katrina and Rita (2005). Journal of Geophysical Research. 2008;**113**: D15108

[3] Srock AF, Bosart LF. Heavy Precipitation Associated with Southern Appalachian Cold-Air Damming and Carolina Coastal Frontogenesis in Advance of Weak Landfalling Tropical Storm Marco (1990). Monthly Weather Review. 2009;**137**:2448-2470

[4] Xue H, Feingold G, Stevens B. Aerosol effects on clouds, precipitation, and the organization of shallow cumulus convection. Journal of the Atmospheric Sciences. 2008;**65**:392-406

[5] Jensen JB, Lee S, Krummel PB, Katzfey J, Gogoasa D. Precipitation in marine cumulus and stratocumulus. Part I: Thermodynamic and dynamic observations of closed cell circulations and cumulus bands. Atmospheric Research. 2000;**54**:117-155

[6] Tompkins AM. Organization of tropical convection in low vertical wind shears: The role of cold pools. Journal of the Atmospheric Sciences. 2001;**58**:1650-1672

[7] Eastin MD, Gardner TL, Link MC, Smith KC. Surface cold pools in the outer rainbands of Tropical Storm Hanna (2008) near landfall. Monthly Weather Review. 2012;**140**:471-491

[8] Markowski PM, Richardson YP. Mesoscale Meteorology in Midlatitudes. John Wiley and Sons; 2010. p. 430

[9] Willoughby HE, Marks Jr FD, Feinbergand RJ, 1984: Stationary and moving convective bands in asymmetric hurricanes. Journal of the Atmospheric Sciences, **41**: 3189-3211

[10] Montgomery MT, Kallenbach RJ. A theory for vortex Rossby-waves and its application to spiral bands and intensity changes in hurricanes. Quarterly Journal of the Royal Meteorological Society. 1997;**123**:435-465

[11] Powell MD. Boundary layer structure and dynamics in outer hurricane rainbands. Part I: Mesoscale rainfall and kinematic structure. Monthly Weather Review. 1990a;**118**:891-917

[12] Powell MD. Boundary layer structure and dynamics in outer hurricane rainbands. Part II: Downdraft modification and mixed layer recovery. Monthly Weather Review. 1990b; **118**:918-938

[13] Knupp KR, Walters J, Biggerstaff M. Doppler profiler and radar observations of boundary layer variability during the landfall of Tropical Storm Gabrielle. Journal of the Atmospheric Sciences. 2006;**63**:234-251

[14] Forbes GS, Anthes RA, Thomson DW. Synoptic and mesoscale aspects of an Appalachian ice storm associated with cold-air damming. Monthly Weather Review. 1987;**115**:564-591

[15] Atallah EH, Bosart LF. The extratropical transition and precipitation distribution of Hurricane Floyd (1999). Monthly Weather Review. 2003;**131**:1063-1081

[16] Bosart LF, Lackmann GM. Postlandfall tropical cyclone reintensification in a weakly baroclinic environment: A case study of Hurricane David (September 1979). Monthly Weather Review. 1995;**123**:3268-3291

[17] Klein PM, Harr PA, Elsberry RL. Extratropical transition of western North Pacific tropical cyclones: An overview and conceptual model of the transformation stage. Weather and Forecasting. 2000;**15**:373-395

[18] Jones SC, and Coauthors, 2003: The extratropical transition of tropical cyclones: Forecast challenges, current understanding, and future directions. Weather and Forecasting, **18**: 1052-1092

[19] Snodgrass ER, Di Girolamo L, Rauber RM. Precipitation characteristics of trade wind clouds during RICO derived from radar, satellite, and aircraft measurements. Journal of Applied Meteorology and Climatology. 2009;**48**:464-483

[20] Tan Z–M, Wu R. Helicity dynamics of atmospheric flow. Advances in Atmospheric Sciences. 1994;**11**:175-188

[21] Ma L–M, Bao X–W. Parametrization of planetary boundary-layer height with helicity and verification with tropical cyclone prediction. Boundary-Layer Meteorology. 2016;**160**: 569-593

[22] Lilly DK. The structure, energetics, and propagation of rotating convective storms. Part II: Helicity and storm stabilization. Journal of the Atmospheric Sciences. 1986;**43**:126-140

[23] Weisman ML, Rotunno R. On the use of vertical wind shear versus helicity in interpreting supercell dynamics. Journal of the Atmospheric Sciences. 2000;**57**:1452-1472

[24] Fei S, Tan Z. On the Helicity dynamics of Severe Convective Storms. Advances in Atmospheric Sciences. 2001;**18**:67-86

[25] Hendricks EA, Montgomery MT, Davis CA. The role of "vortical" hot towers in the formation of Tropical Cyclone Diana (1984). Journal of the Atmospheric Sciences. 2004;**61**: 1209-1232

[26] Wu W-S, Lilly DK, Kerr RM. Helicity and thermal convection with shear. Journal of the Atmospheric Sciences. 1992;**49**:1800-1809

[27] Montgomery MT, Bell MM, Aberson SD, et al. Hurricane Isabel (2003): new insights into the physics of intense storms. Part I. Bulletin of the American Meteorological Society. 2006; **87**:1335-1347

[28] Molinari J, Vollaro D. Distribution of Helicity, CAPE, and Shear in Tropical Cyclones. Journal of the Atmospheric Sciences. 2010;**67**:274-284

[29] Davis CA, Jones SC, Riemer M. Hurricane vortex dynamics during Atlantic extratropical transition. Journal of the Atmospheric Sciences. 2008;**65**:714-736

[30] Kain JS. The Kain–Fritsch convective parameterization: An update. Journal of Applied Meteorology. 2004;**43**:170-181

[31] Ma L-M, Tan Z-M. Improving the behavior of the cumulus parameterization for tropical cyclone prediction: Convection trigger. Atmospheric Research. 2009;**92**:190-211

[32] Hong S-Y, Noh Y, Dudhia J. A new vertical diffusion package with an explicit treatment of entrainment processes. Monthly Weather Review. 2006;**134**:2318-2341

[33] Noh Y, Cheon WG, Hong SY, et al. Improvement of the K-profile Model for the Planetary Boundary Layer based on Large Eddy Simulation Data. Boundary-Layer Meteorology. 2003;**107**:401-427

[34] Hong SY, Pan HL. Nonlocal boundary layer vertical diffusion in a medium-range forecast model. Monthly Weather Review. 1996;**124**:2322-2339

[35] Skamarock WC, Klemp JB, Dudhia J, Gill DO, Barker DM, Duda M, Huang X-Y, Wang W, Powers JG, 2008: A Description of the Advanced Research WRF Version 3. NCAR Technical Note

[36] Mlawer EJ, Taubman SJ, Brown PD, Iacono MJ, Clough SA. RRTM, a validated correlated-k model for the longwave. Journal of Geophysical Research. 1997;**102**:16 663-16 682

[37] Dudhia J. Numerical study of convection observed during the winter monsoon experiment using a mesoscale two dimensional model. Journal of the Atmospheric Sciences. 1989;**46**:3077-3107

[38] Ma L-M, Tan Z-M. Tropical cyclone initialization with dynamical retrieval from a modified UWPBL model. Journal of the Meteorological Society of Japan. 2010;**88**:827-846

[39] Moffat HK. The degree of knottedness of tangled vortex lines. Journal of Fluid Mechanics. 1969;**35**:117-129

[40] Klimowski BA, Przybylinski RW, Schmocker G, Hjelmfelt MR. Observations of the formation and early evolution of bow echoes. Preprints, 20th Conf. on Severe Local Storms, Orlando, FL, Amer. Meteor. Soc.; 2000. 44-47

[41] Schmocker GK, Przybylinski RW, Rasmussen EN. The severe bow echo event of 14 June 1998 over the mid-Mississippi Valley region: A case of vortex development near the intersection of a preexisting boundary and a convective line. Preprints, 20th Conf. on Severe Local Storms, Orlando, FL, Amer. Meteor. Soc; 2000. 169-172

[42] Miles JW, Howard LN. Note on heterogeneous shear flow. Journal of Fluid Mechanics. 1964;**20**:331-336

[43] Carbone RE. A severe frontal rainband. Part I: Stormwide hydrodynamic structure. Journal of the Atmospheric Sciences. 1982;**39**:258-279

[44] Lee BD, Wilhelmson RB. The numerical simulation of non-supercell tornadogenesis. Part I: Initiation and evolution of pretornadic misocyclone and circulations along a dry outflow boundary. Journal of the Atmospheric Sciences. 1997;**54**:32-60

[45] Means LL. A study of the mean southerly wind—Maximum in low levels associated with a period of summer precipitation in the Middle West. Bulletin of the American Meteorological Society. 1954;**35**:166-170

[46] Maddox RA. Large-scale meteorological conditions associated with midlatitude, mesoscale convective complexes. Monthly Weather Review. 1983;**11**:1475-1493

[47] Johns RH, Doswell CA III. Severe local storms forecasting. Weather and Forecasting. 1992;**7**:588-612

[48] Coniglio MC, Elmore KL, Kain JS, Weiss S, Xue M, Weisman ML. Evaluation of WRF model output for severe-weather forecasting from the 2008 NOAA Hazardous Weather Testbed Spring Experiment. Weather and Forecasting. 2010;**25**:408-427

[49] Augustine JA, Caracena F. Lower-tropospheric precursors to nocturnal MCS development over the central United States. Weather and Forecasting. 1994;**9**:115-135

[50] Trier SB, Davis CA, Ahijevych DA, et al. Mechanisms supporting long-lived episodes of propagating nocturnal convection within a 7-day WRF model simulation. Journal of the Atmospheric Sciences. 2006;**63**:2437-2461

[51] Barnes GM, Garstang M. Subcloud layer energetics of precipitating convection. Monthly Weather Review. 1982;**110**:102-117

[52] Barnes GM, Sieckman K. The environment of fast- and slow-moving tropical mesoscale convective cloud lines. Monthly Weather Review. 1984;**112**:1782-2601

[53] Skwira GD, Schroeder JL, Peterson RE. Surface observations of landfalling hurricane rainbands. Monthly Weather Review. 2005;**133**:454-465

[54] Kimball SK. A modeling study of hurricane landfall in a dry environment. Monthly Weather Review. 2006;**134**:1901-1918

[55] Gilmore MS, Wicker LJ. the influence of midtropospheric dryness on supercell morphology and evolution. Monthly Weather Review. 1998;**126**:943-958

[56] McCaul EW Jr, Cohen C. The impact on simulated storm structure and intensity of variations in the mixed layer and moist layer depths. Monthly Weather Review. 2002;**130**: 1722-1748

[57] Bryan GH, Knievel JC, Parker MD. A multimodel assessment of RKW theory's relevance to squall-line characteristics. Monthly Weather Review. 2006;**134**:2772-2792

[58] Romine GS, Wilhelmson RB. Finescale spiral band features within a numerical simulation of Hurricane Opal (1995). Monthly Weather Review. 2006;**134**:1121-1139

[59] Weckwerth TM, Wakimoto RM. The initiation and organization of convective cells atop a cold air outflow boundary. Monthly Weather Review. 1992;**120**:2169-2187

[60] Atkins NT, Laurent MS. Bow echo mesovortices, Part I: Processes that influence their damaging potential. Monthly Weather Review. 2009;**137**:1497-1513

[61] Scorer RS. Theory of airflow over mountains: II—The flow over a ridge. Quarterly Journal of the Royal Meteorological Society. 1953;**79**:70-83

[62] Tan Z–M, Zhang F, Rotunno R, Snyder C. Mesoscale Predictability of Moist Baroclinic Waves: Experiments with Parameterized Convection. Journal of the Atmospheric Sciences. 2004;**61**:1794-1804

[63] Krishnamurti TN, Pattnaik S, Stefanova L, Vijaya Kumar TSV, Mackey BP, O'Shay AJ, Pasch RJ. The hurricane intensity issue. Monthly Weather Review. 2005;**133**:1886-1912

[64] Saltzman B. Largescale atmospheric energetics in the Wave-Number Domain. Reviews of Geophysics and Space Physics. 1970;**8**:289-302

[65] Snyder C, Hamill TM, Trier S. Linear evolution of forecast error covariances in a quasi-geostrophic model. Monthly Weather Review. 2003;**131**:189-205

[66] Andre JC, Lesieur M. Influence of helicity on high Reynolds number isotropic turbulence. Journal of Fluid Mechanics. 1977;**81**:187

[67] Tsinober A, Levich E. On the helical nature of three dimensional coherent structures in turbulent flows. Physics Letters. 1983;**99A**:321

[68] Black ML, Gamache JF, Marks Jr FD, et al. Eastern Pacific Hurricanes Jimena of 1991 and Olivia of 1994: The effect of vertical shear on structure and intensity. Monthly Weather Review. 2002;**130**:2291-2312

[69] Houze RA Jr. Orographic effects on precipitating clouds. Reviews of Geophysics. 2012;**50**: RG1001. DOI: 10.1029/2011RG000365

IntechOpen